ARTICLE IN PRESS
JID: JMAA [m5+;June 27, 2020;4:26]

Available online at www.sciencedirect.com

ScienceDirect

Journal of Magnesium and Alloys xxx (xxxx) xxx

www.elsevier.com/locate/jma

Full Length Article

Enhancing the strain hardening and ductility of Mg-Y alloy by introducing stacking faults

Kang Wei, Lirong Xiao, Bo Gao, Lei Li, Yi Liu, Zhigang Ding, Wei Liu, Hao Zhou*, Yonghao Zhao*

Nano and Heterogeneous Materials Center, School of Materials Science and Engineering, Nanjing University of Science and Technology, Nanjing 210094, China

Received 24 July 2019; received in revised form 16 September 2019; accepted 19 September 2019
Available online xxx

Abstract

Due to the insufficient slip systems, Mg and its alloys exhibit poor ductility during plastic deformation at room temperature. To solve this problem, alloying is considered as a most effective method to improve the ductility of Mg alloys, which attracts wide attentions of industries. However, it is still a challenge to understand the ductilization mechanism, because of the complicated alloying elements and their interactions with Mg matrix. In this work, pure Mg and Mg-Y alloys were comparatively studied to investigate the effect of Y addition on microstructure evolution and mechanical properties. A huge increase of uniform elongation, from 5.3% to 20.7%, was achieved via only 3 wt% addition of yttrium. TEM results revealed that the only activated slip system in pure Mg was basal <*a*> slip, led to its poor ductility at room temperature. In contrast, a large number of stacking faults and non-basal dislocations with <*c*> component were observed in the deformed Mg-Y alloy, which was proposed as the main reason for significant improvement of strain hardening and ductility. High resolution TEM indicated that most of the stacking faults were I1 and I2 intrinsic faults, which played a critical role in improving the ductility of Mg-Y alloy. Addition of Y into Mg alloy decreased the stacking fault energy, which induced high density stacking faults in the grain interior.

Keywords: Magnesium alloys; Ductility; Stacking faults; Non-basal slip; Transmission electron microscopy.

1. Introduction

As the lightest metallic materials, magnesium and its alloys have great potential for structural applications in many fields, such as automotive, aerospace, and electronic industries [1–3]. However, the activable slip systems in hexagonal close-packed (hcp) structural materials are not enough for the uniform plastic deformation at room temperature, which limits the commercial applications of wrought magnesium alloys [4]. The most popular strategy to solve this problem was to introduce more slip systems in Mg alloys. Especially, the introduction of pyramidal <*c*+*a*> slips provided five more independent slip systems required for homogeneous deformation of polycrystals, which played a critical role in enhancing the crystal plasticity of Mg alloys [5,6]. It has been reported that there are several methods to activate <*c*+*a*> slips in Mg, such as grain refinement [7], alloying design [8,9], and hot deformation [10–12]. Among them, alloying was considered as the most convenient method because of its low technical demand and production cost. Addition of Rare earth (RE) elements into Mg alloys was found to not only promote the weakening of texture, but also increase the activation of non-basal slips, which improved their ductility at room temperature remarkably [13,14].

However, the mechanism of ductilization is complicated, because it is difficult to obtain direct evidence of interaction between alloying elements and Mg matrix. Wang et al. [15] performed an in-situ tensile experiments on Mg-3Y

* Corresponding authors.
E-mail addresses: hzhou511@njust.edu.cn (H. Zhou), yhzhao@njust.edu.cn (Y. Zhao).

https://doi.org/10.1016/j.jma.2019.09.015

alloy using three dimensional X-ray diffraction. They found that the addition of Y element promoted the activity of prismatic and pyramidal slip systems. Additionally, RE addition was proposed to reduce the basal plane stacking fault energy (SFE) of Mg, which was coincident with the results of density functional theory (DFT) simulations [16–18]. Sandlöbes et al. [14,16] found that a large number of I1 stacking faults generated in a deformed Mg-RE alloys. They believed that the I1 stacking faults acted as heterogeneous sources for nucleation of pyramidal <c+a> slips. However, a minority controversial views claimed that there was no direct relationship between the <c+a> slips and stacking faults [19,20]. Zhang et al. [20] investigated the tensile and compressive behaviors of the fine-grained Mg-Y alloy. Instead of <c+a> dislocations, many stacking faults were observed in the deformed samples, which was believed to play negative roles in impeding non-basal slips, and consequently to deteriorate the formability of Mg alloys [5,21,22]. In order to solve this controversy, more detailed investigations on the deformation mechanism of Mg-RE alloys were carried out in this work. The microstructure evolution and mechanical properties of pure Mg and Mg-Y alloy were comparatively studied, which revealed the effect of Y addition on the deformation mechanism of Mg alloys.

2. Material and methods

Ingots of Mg-3Y (wt%) alloy were prepared from a high purity Mg (99.99%) metal and a Mg-25Y (wt%) master alloy in an electric-resistant furnace under a mixed protective gas of Ar and SF_6 that has a volume ratio of 100:1(The details of alloy preparation have been reported in Ref. [23]). The as-cast ingots of pure Mg and Mg-3Y were homogenized in a vacuum furnace at 450 °C for 20 h and at 530 °C for 12 h, respectively, which were followed by water quenching to room temperature. Rolling deformation was performed on the two materials to eliminate the casting defects, which deformed the samples to a thickness reduction of 10%. The rolled samples were fully annealed for recrystallization at 325 °C (pure Mg) and at 500 °C (Mg-3Y) alloy, respectively. Dog-bone shaped specimens with a gauge length of 10 mm and width of 2.5 mm were cut from the annealed samples for tensile testing. The uniaxial tensile testing was performed on a walter + bai mechanical testing machine (LFM-20kN) with a strain rate of 2×10^{-3} s^{-1} at room temperature. The samples for TEM observations were obtained from the tensile specimens which interrupt at an engineering strain of ~4%. The samples for optical microscopy observation were ground with sandpaper of 320, 800, 1200 and 2000 grits, and then polished by woolen cloth to a mirror finish. To observe microstructure under optical microscope, samples were etched by lab-prepared solution comprised of 95 ml ethyl alcohol and 5 ml nitric acid.

Cross-sectional TEM specimens were cut perpendicular to the tensile direction and gently polished to a thickness of ~25 μm. Perforation by ion milling (Gatan PIPS 691) was carried out on a cold stage (~−50 °C) with low angle (5°) and low energy ion beam (4 KeV). TEM observations were conducted on an FEI-Tecnai G2 20 LaB6 microscope operated at an accelerating voltage of 200 kV, and the high-resolution TEM (HRTEM) observations were carried out on a Titan G2 60-300 at 300 kV.

3. Results and discussions

As shown in Fig. 1a and b, the annealed samples of pure Mg and Mg-3Y alloy exhibit similar microstructure, which have average grain sizes of ~196 μm and ~199 μm, respectively. Equivalent densities of annealing twins exist in some grains of both specimens as marked by the white arrows. Twins are frequently observed in many Mg alloys, which is an important deformation mode to improve ductility similar to dislocations [24]. However, the contribution of twinning to plasticity is very limited, because it only allows simple shear in one direction [25]. Fig. 1c shows the tensile stress–strain curves of the annealed pure Mg and Mg-Y alloy. The yield stress (YS, 0.2% proof stress) and ultimate tensile strength (UTS) of the materials are very close to each other, which are ~50 MPa and ~130 MPa, respectively. Interestingly, the Mg-3Y alloy exhibits a four times higher uniform elongation (~21 ± 1.2%) than that of pure Mg (~5 ± 0.5%). Note that, pure Mg and Mg-3Y alloy specimens contain almost identical grain size and twinning density. Thus, it is reasonable to propose that such significant ductilization of Mg-Y alloy is mainly due to the addition of Y element. Fig. 1d shows that the strain-hardening rate of the pure Mg decreased drastically after 5% of tensile strain. While, it is also found that the work hardening capability increased with addition of Y, which helps with retaining ductility of Mg. Previous researches believed that the ductilization of Mg-RE alloys were resulted from the weakening of basal plane texture, which was beneficial to activate non-basal slip systems in Mg-RE alloys [14,26]. It indicated that dislocation type was the most fundamental issue for improving ductility of Mg alloys [13]. Therefore, the types and configurations of dislocations in grain interior of pure Mg and Mg-Y alloy were investigated intensively.

To explore the underlying ductilization mechanism of Mg-Y alloy, detailed TEM characterizations (more than 30 grains for each sample) were performed on the pure Mg and Mg-Y samples subjected to a same strain of ~4%. According to the "$\boldsymbol{g}\bullet\boldsymbol{b}$" criterion, dislocations are invisible when $\boldsymbol{g}\bullet\boldsymbol{b}=0$, where $\boldsymbol{g}$ and $\boldsymbol{b}$ represent diffraction vectors and Burgers vectors, respectively. In other words, <a> dislocations with $\boldsymbol{b}={}^1/_3$<11-20> are invisible if the two beam condition is set as $\boldsymbol{g}=0002$, and the <c> dislocations with $\boldsymbol{b}$=<0001> are mostly unable to be observed in the condition of $\boldsymbol{g}=$0-110. If the dislocations can be observed in the images of above two beam conditions, they will be determined as the <c+a> dislocations with $\boldsymbol{b}={}^1/_3$<11-23> [27,28].

Fig. 2a–c show the microstructures of a deformed pure Mg observed near the [2-1-10] zone axis. The two-beam diffraction conditions were set as $\boldsymbol{g}=0002$ and $\boldsymbol{g}=$0-110, as shown in Fig. 2a and b, respectively. A twin marked by the white pentagram is selected as the label structure to determine the accurate positions of observation area. All the dislocations can only be observed in the condition of $\boldsymbol{g}=$0-110 (Fig. 2b

Please cite this article as: K. Wei, L. Xiao and B. Gao et al., Enhancing the strain hardening and ductility of Mg-Y alloy by introducing stacking faults, Journal of Magnesium and Alloys, https://doi.org/10.1016/j.jma.2019.09.015

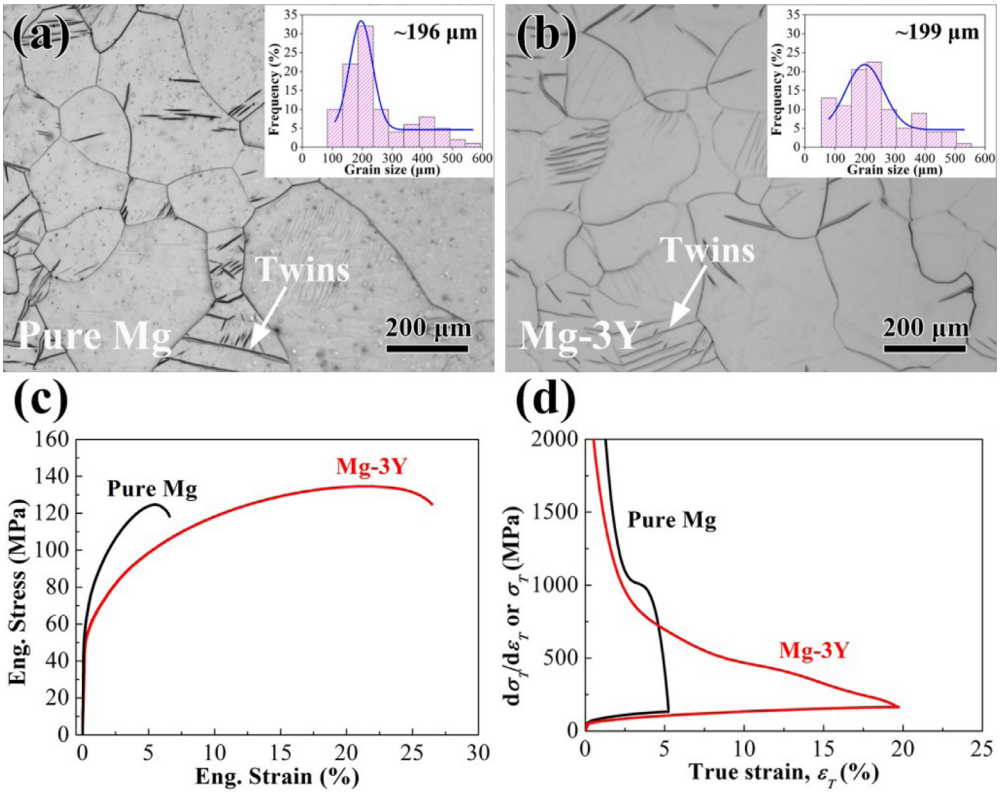

Fig. 1. Microstructures and mechanical properties of as-received samples: (a) and (b) Optical microscopy images of Pure Mg and Mg-3Y, respectively. The insets are grain size distribution charts; (c) Tensile curves of nominal stress vs. strain; and (d) True stress–strain and strain hardening curves from tensile tests.

and c), which indicates that these dislocations in pure Mg are mostly basal <*a*> type dislocations, as marked by yellow arrows. It is generally accepted that basal slip system is easier to be activated than other slip systems in pure Mg, because the resolved shear stress (CRSS) of basal slip is much lower than that of non-basal slips [29]. Therefore, basal slip is dominated in the tensile deformation of pure Mg, resulting in poor ductility at room temperature.

Fig. 2d–f show the TEM images of the Mg-Y alloy near the direction of [2-1-10] zone axis. A grain boundary marked by a white pentagram pattern is selected as the label structure. Besides basal <*a*> dislocations shown in Fig. 2e, numerous non-basal dislocations with <*c*> component were observed in the image with $\boldsymbol{g}$=0002 (Fig. 2d). The enlarged image in Fig. 2f shows that these visible <*c*> type dislocations are distributed randomly as marked by the blue arrows. Previous experimental and computational studies have revealed that the <*c*+*a*> dislocations can be dissociated into perfect <*a*> dislocations and <*c*> partials during the deformation of Mg-RE alloys [5,13,17,30,31]. Thus, most of non-basal <*c*> dislocations shown in Fig. 2f are decomposed from pyramidal <*c*+*a*> dislocations. Solute-enhanced <*c*+*a*> slip activity accommodates the *c*-axis strain of hexagonal crystals, providing enough independent deformation systems to satisfies the Von Mises criteria, and improves the ductility of Mg-Y alloy significantly [13]. Moreover, it should be noted that there are many straight lines parallel to the basal plane trace in Fig. 2f, which are most likely nano-spaced I1 stacking faults (I1 SFs, marked by the red dashed ellipses) bounded by $^1/_6$<20-23> Frank partials. The combined microstructural features of <*c*> type dislocations and I1 faults have been reported in other magnesium-rare earth alloys, such as in Ref. [16,30]. It indicates that non-basal <*c*> dislocations and I1 stacking faults are observed in most grains (more than 90%), co-existing with basal <*a*> dislocations. The related DFT calculation results showed that the intrinsic I1 SFE was significantly decreased due to the addition of Y, which promoted the generation of I1 SFs. It was also proposed that I1 faults acted as heterogeneous nucleation source for the non-basal slip [16]. Moreover, Ding et al. [17] proposed that alloying with Y element could increase the range of the potential-energy surface and decrease both unstable and stable SFE, which reasonably explained the high amount of non-basal <*c*> dislocations and remarkable improvement of ductility in Mg-Y alloy.

HRTEM observations were performed to investigate the detailed structure of stacking faults (SFs). As shown in Fig. 3a and b, a high density of basal SFs (marked by the yellow arrows) are observed in the grain interior of Mg-3Y alloy. The spacing of SFs is in the range of 3–10 nm. Meanwhile, some bright streaks (indicated by the white arrows) appear in the fast Fourier transform (FFT) pattern (Insert in Fig. 3b), which is consistent with the diffraction shape effect of SFs on the basal plane. In order to identify the accurate types of SFs and their bounding dislocations, atomic-scaled observations

Please cite this article as: K. Wei, L. Xiao and B. Gao et al., Enhancing the strain hardening and ductility of Mg-Y alloy by introducing stacking faults, Journal of Magnesium and Alloys, https://doi.org/10.1016/j.jma.2019.09.015

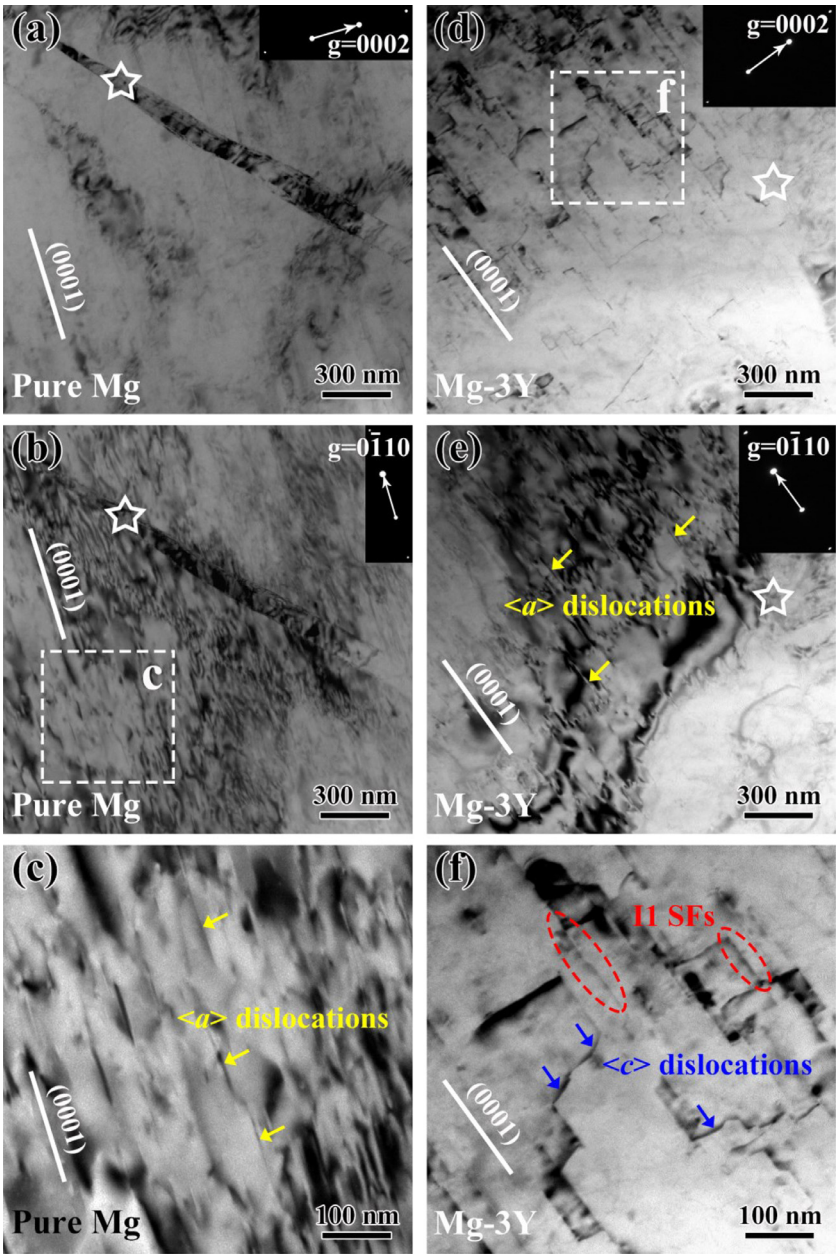

Fig. 2. TEM images in two-beam condition near the [2-1-10] zone axis: (a) and (b) Pure Mg viewed under $\boldsymbol{g}=0002$ and $\boldsymbol{g}=0\text{-}110$, respectively; (d) and (e) Mg-Y alloy viewed under $\boldsymbol{g}=0002$ and $\boldsymbol{g}=0\text{-}110$, respectively; (c) and (f) Enlarged images of selected area in (b) and (d), respectively; The white straight lines highlight the trace of (0001) basal plane.

were carried out on the aberration-corrected TEM operated at 300 kV. Interestingly, all of the SFs observed in Mg-Y alloy are intrinsic faults, while no extrinsic faults are found in the alloy. Fig. 3c and d show the atomic scaled TEM images of I1 faults, in which a Burgers circuit is drawn around the dislocation core. The start point D does not overlap with the finish point E, which indicates that vector DE (marked by the red arrow heads in Fig. 3d) is the Burgers vector of Frank partial dislocation ($\boldsymbol{b}=1/6\langle 20\text{-}23\rangle$). Similarly, the atomic-scaled structures of I2 faults are also characterized, as shown in Fig. 3e and f. The Burgers vector of its partial dislocation is $1/3\langle 10\text{-}10\rangle$, as illustrated by the Burgers circuit in Fig. 3f.

As shown in Fig. 4, the atomic models of I1 and I2 faults are established according to the experimental results. It is clear that I1 and I2 faults introduce a thin three-layer and four-layer of face-center cubic (fcc) stacking structure into the hcp matrix, respectively. The 2D atomic model in Fig. 4b shows that the stacking sequence of I1 faults is ABAB**ABC**BCBCB. I1 intrinsic faults can be produced through the convergence of vacancies or interstitials on the basal plane, combined with the shear process of Shockley

Please cite this article as: K. Wei, L. Xiao and B. Gao et al., Enhancing the strain hardening and ductility of Mg-Y alloy by introducing stacking faults, Journal of Magnesium and Alloys, https://doi.org/10.1016/j.jma.2019.09.015

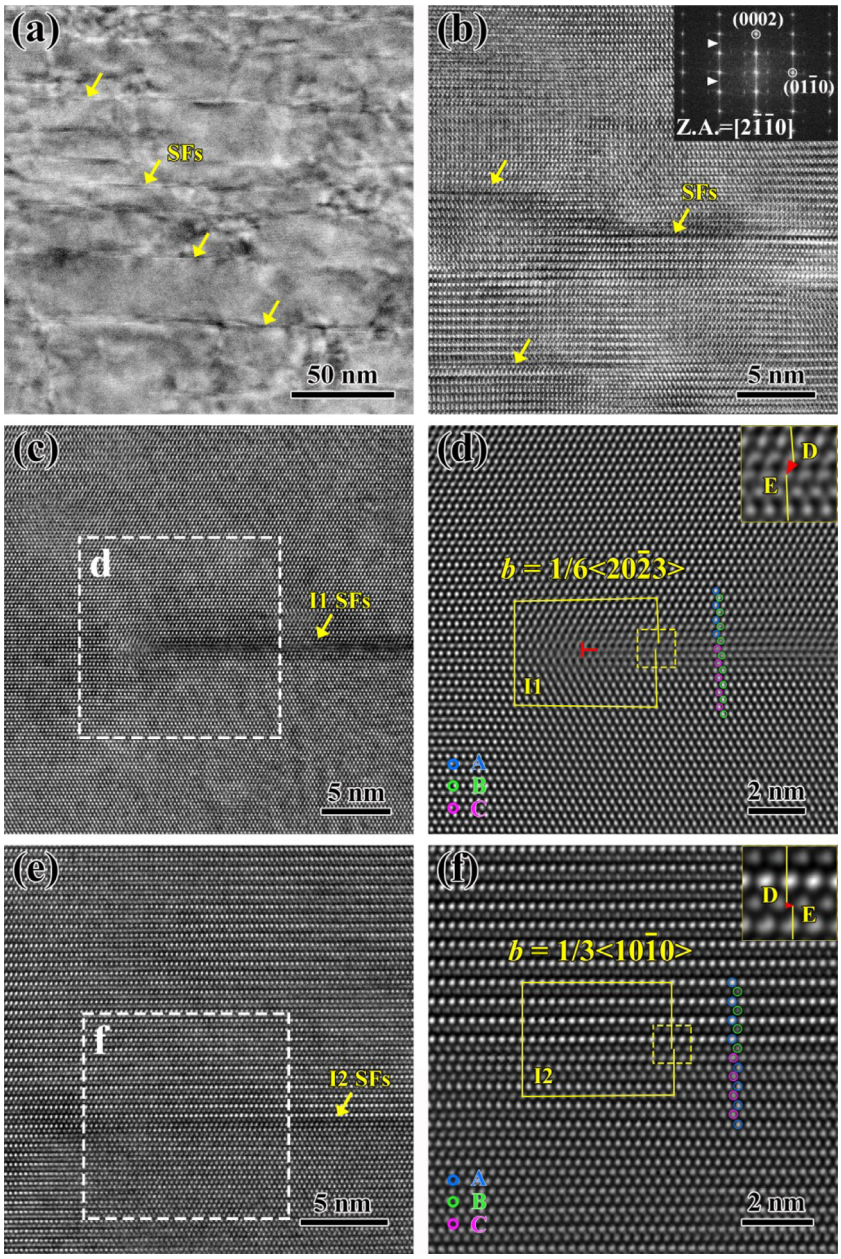

Fig. 3. Microstructures of a deformed grain in Mg-3Y alloy obtained from [2-1-10] axis: (a) and (b) the HRTEM images and corresponding fast Fourier transform (FFT) pattern of stacking faults; (c) and (d) the atomic scaled TEM images of I1 faults bounded by $^1/_6$<20-23> Frank partials; (e) and (f) the atomic scaled TEM images of I2 faults bounded by $^1/_3$<10-10> Shockley partials. Insets in (d) and (f) are the enlarged images of the corresponding square regions denoted by the dash lines, respectively, and red arrow heads highlight the Burgers vectors of the partials. (For interpretation of the references to color in this figure legend, the reader is referred to the web version of this article.)

partial dislocations, thus resulting in I1 faults bounded by $^1/_6$<20-23> Frank partials [32]. The corresponding dislocation reaction is described in Eq. (1). I1 stacking faults act as heterogeneous nucleation sources for perfect <c+a> dislocations [16]. Agnew et al. [33] proposed that the source mechanism was energetically conceivable for a wide range of fault geometries. Moreover, the glissile pyramidal <c+a> dislocations were proposed to generate from interactions between sessile Frank partials bounding I1 SFs on basal plane, which enhanced the capacity for plastic flow of the HCP crystal materials [34]. Consequently, I1 SFs have a positive contribution on improving the ductility of Mg-Y alloy in this work.

$$\frac{1}{2} < 0001 > + \frac{1}{3} < 10\bar{1}0 > \rightarrow \frac{1}{6} < 20\bar{2}3 > \quad (1)$$

Fig. 4d reveals the 2D atomic structure of I2 faults yielding the sequence of ABAB**ABCA**CACA. It is generally accepted that I2 faults are dissociated from the perfect basal <a> dislocations. Its intrinsic dislocation reaction is represented in Eq. (2). Basically, I2 faults are bounded by Shockley partials ($\boldsymbol{b}$ = $^1/_3$<10-10>), which remain glissile on basal planes to accommodate the basal strain. Meanwhile, the basal partials

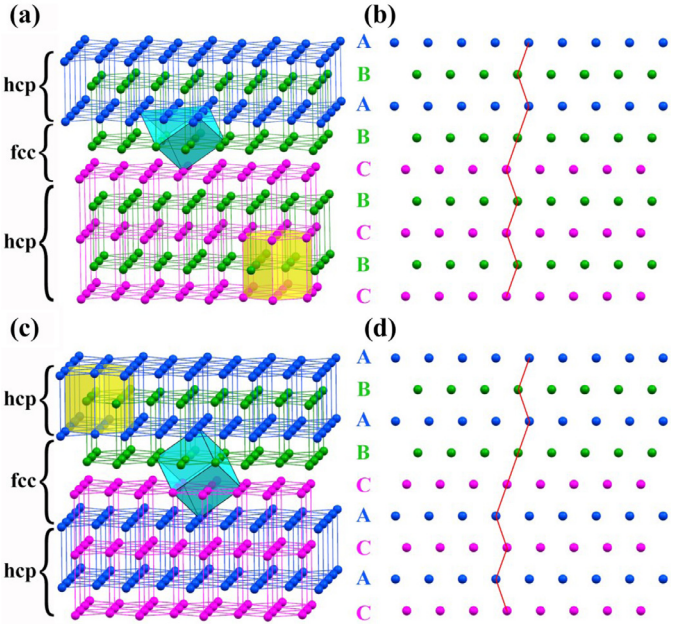

Fig. 4. Atomic models of stacking faults in Mg-Y alloy: (a) and (b) the 3D and 2D models of I1 faults, respectively; (c) and (d) the 3D and 2D models of I2 faults, respectively.

provide Shockley shear for nucleation of perfect <c+a> dislocations, as illustrated by Eq. (1), leading to a higher activity of pyramidal dislocation slip. Thus, both the I1 and I2 faults are beneficial to improve the ductility of Mg-Y alloy.

$$\frac{1}{3}<11\bar{2}0>\rightarrow\frac{1}{3}<10\bar{1}0>+\frac{1}{3}<01\bar{1}0> \quad (2)$$

Based on the experimental results, the corresponding SFE of γ, can be calculated by the following formula [16,35]:

$$\gamma=\frac{Gb^2}{8\pi d}\frac{2-\nu}{1-\nu}\left(1-\frac{2\nu}{2-\nu}\cos 2\beta\right) \quad (3)$$

Where G represents the shear modulus, ν the Poisson's ratio, β the angle between the partial dislocations; b is the magnitude of the Burgers vector of the partials, and d is the measured width of the stacking faults. The values used for pure Mg ($G=17$ GPa, ν=0.35, $b=0.186$ nm for Shockley partials; $b=0.320$ nm for Frank partials) were also adopted for the solid solution Mg-Y alloys [36].

The average I1 and I2 SFE of Mg-3Y determined via formula (3) amounts to 3.7 ± 0.5 mJ m^{-2} and 3.4 ± 0.6 mJ m^{-2}, respectively, which are distinctly lower than the basal SFEs (experimental measurements, by TEM analysis: >50 mJ m^{-2}) of pure Mg [16]. Recently, extensive DFT studies have been carried out to investigate the effect of alloying RE elements on the SFEs of binary Mg alloys [37–40]. The calculated results further reveal that slight additions of Y into Mg can reduce the SFEs significantly (I1 SFE: from 18–21 to 4–9 mJ m^{-2}, I2 SFE: from 30–38 to 14–23 mJ m^{-2}), which are qualitatively coincide with the experimental results in our study. Physical features controlling the SFE with alloying Y element have been considered in previous works. Wu et al. [37] suggested that solute Y atoms led to charge redistribution of matrix Mg atoms, and the disturbance of the pseudo-atom bonds in the pristine lattice of Mg-Y caused the reduction of SFE. In addition, Zhang et al. [38] pointed out that changing of the SFE was expected to be related to the ionization energy and atomic radius of solute atoms. Substituting Mg atom by alloying Y atom with lower 1st ionization energy and bigger atomic radius tended to induce lattice expansion, which led to reducing of SFE.

4. Conclusions

The microstructure evolution and mechanical properties of pure Mg and Mg-Y have been comparatively studied. A huge enhancement of uniform elongation, from 5.3% to 20.7%, was achieved via only 3 wt% of Y addition. The key findings are summarized as follows:

(1) Basal slip is dominated in the tensile deformation of pure Mg, resulting in poor ductility at room temperature. In contrast, besides basal <a> dislocations, numerous SFs and non-basal dislocations with <c> component exist in the Mg-Y alloy, which provides sufficient slip systems to achieve a homogeneous plastic deformation.
(2) All of the SFs observed in Mg-Y alloy are I1 and I2 intrinsic faults, while no extrinsic faults are found in the alloy. The I1 and I2 faults are bounded by Frank partials ($\boldsymbol{b}=1/6<20\text{-}23>$) and Shockley partials ($\boldsymbol{b}=1/3<10\text{-}10>$), respectively. The significant decrease of SFE is proposed as the main reason for the formation of high density SFs.

Acknowledgments

This work was supported by the National Key R&D Program of China (2017YFA0204403), National Natural Science Foundation of China (51601003, 51901103), and the Fundamental Research Funds for the Central Universities (30918011342). The authors wish to express their appreciation to the Jiangsu Key Laboratory of Advanced Micro&Nano Materials and Technology. TEM experiments were performed at the Materials Characterization and Research Center of Nanjing University of Science and Technology.

References

[1] J.H. Zhang, S.J. Liu, R.Z. Wu, L.G. Hou, M.L. Zhang, J. Magnes. Alloys 6 (2018) 277–291.
[2] Y.T. Tang, C. Zhang, L.B. Ren, W. Yang, D.D. Yin, G.H. Huang, H. Zhou, Y.B. Zhang, J. Magnes. Alloys 7 (2019) 522–528.
[3] H. Zhou, G.M. Cheng, X.L. Ma, W.Z. Xu, S.N. Mathaudhu, Q.D. Wang, Y.T. Zhu, Acta Mater. 95 (2015) 20–29.
[4] J.P. Weiler, J. Magnes. Alloys 7 (2019) 297–304.
[5] Z.X. Wu, W.A. Curtin, Nature 526 (2015) 62–67.
[6] L.P. Zhong, Y.J. Wang, Y.C. Dou, J. Magnes. Alloys 7 (2019) 637–647.
[7] L.R. Xiao, X.F. Chen, Y. Cao, H. Zhou, X.L. Ma, D.D. Yin, B. Ye, X.D. Han, Y.T. Zhu, Scr. Mater. 177 (2020) 69–73.
[8] K.K. Alaneme, E.A. Okotete, J. Magnes. Alloys. 5 (2017) 460–475.

[9] L.R. Xiao, Y. Cao, S. Li, H. Zhou, X.L. Ma, L. Mao, X.C. Sha, Q.D. Wang, Y.T. Zhu, X.D. Han, Acta Mater. 162 (2019) 214–225.
[10] A. Javaid, F. Czerwinski, J. Magnes. Alloys. 7 (2019) 27–37.
[11] A. Hadadzadeh, M.A. Wells, J. Magnes. Alloys. 5 (2017) 369–387.
[12] S.A. Sani, G.R. Ebrahimi, H. Vafaeenezhad, A.R. Kiani-Rashid, J. Magnes. Alloys. 6 (2018) 134–144.
[13] K. Luo, L. Zhang, G.H. Wu, W.C. Liu, W.J. Ding, J. Magnes. Alloys. 7 (2019) 345–354.
[14] S. Sandlöbes, Z. Pei, M. Friák, L.F. Zhu, F. Wang, S. Zaefferer, D. Raabe, J. Neugebauer, Acta Mater. 70 (2014) 92–104.
[15] L.Y. Wang, Z.H. Huang, H.M. Wang, A. Maldar, S.B. Yi, J.S. Park, P. Kenesei, E. Lilleodden, X.Q. Zeng, Acta Mater. 155 (2018) 138–152.
[16] S. Sandlöbes, M. Friák, S. Zaefferer, A. Dick, S. Yi, D. Letzig, Z. Pei, L.F. Zhu, J. Neugebauer, D. Raabe, Acta Mater. 60 (2012) 3011–3021.
[17] Z.G. Ding, W. Liu, H. Sun, S. Li, D.L. Zhang, Y.H. Zhao, E.J. Lavernia, Y.T. Zhu, Acta Mater. 146 (2018) 265–272.
[18] S.L. Shang, W.Y. Wang, B.C. Zhou, Y. Wang, K.A. Darling, L.J. Kecskes, S.N. Mathaudhu, Z.K. Liu, Acta Mater. 67 (2014) 168–180.
[19] A. Moitra, S.G. Kim, M.F. Horstemeyer, Acta Mater. 75 (2014) 106–112.
[20] D.L. Zhang, H.M. Wen, M.A. Kumar, F. Chen, L.M. Zhang, I.J. Beyerlein, J.M. Schoenung, S. Mahajan, E.J. Lavernia, Acta Mater. 120 (2016) 75–85.
[21] W.W. Jian, G.M. Cheng, W.Z. Xu, C.C. Koch, Q.D. Wang, Y.T. Zhu, S.N. Mathaudhu, Appl. Phys. Lett. 103 (2013) 133108.
[22] X. Wang, L. Jiang, A. Luo, J. Song, Z. Liu, F. Yin, Q. Han, S. Yue, J.J. Jonas, J. Alloy. Compd. 594 (2014) 44–47.
[23] H. Zhou, Q.D. Wang, J. Chen, B. Ye, W. Guo, Trans. Nonferrous Met. Soc. China 22 (2012) 1891–1895.
[24] X.F. Chen, L.R. Xiao, Z.G. Ding, W. Liu, Y.T. Zhu, X.L. Wu, Scr. Mater. 178 (2020) 193–197.
[25] H. Zhou, Q.D. Wang, B. Ye, W. Guo, Mater. Sci. Eng. A 576 (2013) 101–107.
[26] C.Y. Zhao, Z.Y. Li, J.H. Shi, X.H. Chen, T. Tu, Z. Luo, R.J. Zheng, A. Atrens, F.S. Pan, J. Magnes. Alloys. 7 (2019) 672–680.
[27] D.B. Williams, C.B. Carter, Transmission Electron Microscopy: a Textbook for Materials Science, Springer, New York, 2009.
[28] H. Zhou, C.X. Huang, X.C. Sha, L.R. Xiao, X.L. Ma, H.W. Höppel, M. Göken, X.L. Wu, K. Ameyama, X.D. Han, Y.T. Zhu, Mater. Res. Lett. 7 (2019) 376–382.
[29] E. Karakulak, J. Magnes. Allos. 7 (2019) 355–369.
[30] D.L. Zhang, L. Jiang, J.M. Schoenung, S. Mahajan, E.J. Lavernia, Philos. Mag. 95 (2015) 3823–3844.
[31] M.H. Yoo, S.R. Agnew, J.R. Morris, K.M. Ho, Mater. Sci. Eng. A 319–321 (2001) 87–92.
[32] D. Hull, D.J. Bacon, Introduction to Dislocations, fifth ed., Elsevier, Oxford, 2011.
[33] S.R. Agnew, L. Capolungo, C.A. Calhoun, Acta Mater. 82 (2015) 255–265.
[34] S.Q. Zhu, S.P. Ringer, Acta Mater. 144 (2018) 365–375.
[35] Y. Liu, M.P. Liu, X.F. Chen, Y. Cao, H.J. Roven, M. Murashkin, R.Z. Valiev, H. Zhou, Scr. Mater. 159 (2019) 137–141.
[36] Z.Q. Yang, M.F. Chisholm, G. Duscher, X.L. Ma, S.J. Pennycook, Acta Mater. 61 (2013) 350–359.
[37] Y.F. Wu, S. Li, Z.G. Ding, W. Liu, Y.H. Zhao, Y.T. Zhu, Scr. Mater. 112 (2016) 101–105.
[38] J. Zhang, Y.C. Dou, G.B. Liu, Z.X. Guo, Comput. Mater. Sci. 79 (2013) 564–569.
[39] L.L. Tang, Y.H. Zhao, R.K. Islamgaliev, R.Z. Valiev, Y.T. Zhu, J. Alloy. Compd. 721 (2017) 577–585.
[40] Q. Zhang, L. Fu, T.W. Fan, B.Y. Tang, L.M. Peng, W.J. Ding, Physica B 416 (2013) 39–44.

Please cite this article as: K. Wei, L. Xiao and B. Gao et al., Enhancing the strain hardening and ductility of Mg-Y alloy by introducing stacking faults, Journal of Magnesium and Alloys, https://doi.org/10.1016/j.jma.2019.09.015